



## Development of Microstructure on Titanium Implant Surface Using CO<sub>2</sub> Laser Processing

Ali N. Ahmed Hussein<sup>1</sup>, Raghdaa K. Jassim<sup>2</sup>, Rola W. Abdul-Razzaq<sup>3</sup>

<sup>1,3</sup>Lecturers, Prosthetic Dentistry Department, College of Dentistry, University of Baghdad.  
E-mail : ([ali.ahmed@codental.uobaghdad.edu.iq](mailto:ali.ahmed@codental.uobaghdad.edu.iq)), phone number (+9647901228830).

<sup>2</sup>Professor, Department of Prosthetic Dentistry, College of Dentistry, University of Baghdad.  
Bab-Almoadham, P.O. Box 1417, Baghdad, Iraq.

*Received 14/02/2023*

*Accepted in revised form 01/08/2023*

*Published 30/06/2024*

### Abstract:

**Background:** Dental biomaterials made of titanium are commonly used. It depends on the implant surface texture to improve fixation and prevent the unwanted adhesion of bone cells. **This study aimed to** investigate whether continuous laser beam carbon dioxide (CNC - CO<sub>2</sub>) lasers produce specific textures on titanium surfaces with micrometer-sized indentations that influence cell behavior. **Materials and method:** (CNC - CO<sub>2</sub>) red laser device; with a fundamental wavelength of  $\lambda=10600$  nm and power pulses of 34 W were applied, and textures on the surface of titanium discs were achieved. **Results:** Excellent degrees of uniformity and repeatability were achieved for the desired portions of the surface by creating different surface textures. The surface topography and chemical composition of the specimens were investigated by scanning electron microscopy, electron dispersive spectroscopy, X-ray diffraction, and surface roughness measurements. Also, a laser power of 34 watts raised the surface roughness, Ra (1.71 nm), and Rz (1.99 nm). **Conclusion:** Titanium surface textures with unique qualities can be formed in response to an increased heat input. When excessive laser power was used, the measured roughness increased because of instantaneous re-melting. The use of a right continuous-wave (CNC - CO<sub>2</sub>) laser on titanium used in dental implants can form specific surface textures.

**Keywords:** Direct laser texturing (DLT), scanning electron microscopy (SEM), energy-dispersive spectroscopy (EDS), X-ray diffraction (XRD), (BIC) bone-implant contact, atomic force microscopy (AFM).



## 1. Introduction

Several surface modification techniques have been developed to create featured implant surfaces to enhance the mechanical bone-implant interface. <sup>(1)</sup> The CO<sub>2</sub> laser was one of the earliest gas lasers developed in 1964. It includes a discharge tube, an electric-powered pump supply, and numerous optics, such as mirrors, windows, and lenses. <sup>(2)</sup> In CO<sub>2</sub> lasers, CO<sub>2</sub> gas fills the discharge tube and is electrically pumped via DC or AC. CO<sub>2</sub> lasers can generate an infrared output wavelength from 9 to 11 μm; 10.6 μm is the maximum extensively used wavelength. <sup>(3)</sup> Owing to the infrared wavelength, unique substances are used for optical components, silver or gold for mirrors, and germanium or zinc selenite for windows and lenses. When compared with different continuous-wavelength lasers, CO<sub>2</sub> lasers offer excessive performance (5-20%) and excessive output power (0.1-20 kW) so that they can be extensively utilized in material processing, including slicing, drilling, and welding. Furthermore, for excessive power operation over numerous kilowatts, a heat dissipation tool consisting of a water jacket to cool the electrodes might be included. <sup>(4)</sup>

The simplicity of the machine results in a low price, excessive reliability, and device compactness, which might be the principal reasons why CO<sub>2</sub> lasers are precision production workhorses. <sup>(5)</sup> The CO<sub>2</sub> laser offers restricted work in the manufacturing of metallic elements because of its low light absorption coefficient in the infrared region. <sup>(6)</sup>

Laser micromachining has tremendous capability to modify biomaterial surfaces. The implementation of optical surface texturing enables the intake of a large amount of biomaterial surface, for which unique textures and regular dimensions may be replicable, controlled, and sustainable. <sup>(7)</sup> Microgrooves may be created at the surface using a continuous laser beam, and a pulsed laser may be used to create micropits. <sup>(8)</sup> Hu and Ding

(2012): <sup>(9)</sup> compare textures with a width of 150 μm and lines of 40 μm. It was determined that the texture with the highest width was the most critical element affecting topographic properties. The most efficient texture diameter for the studied prostheses of various sizes and textures was in values 100-400 microns as the ultimate width. Different studies have affirmed that the minimum dimension of the textures is 140-200 microns. <sup>(10)</sup>

Pfleging et al. (2015) <sup>(11)</sup> determined a higher adhesion of osteoblasts and a greater even distribution on laser-surface-textured titanium. Better spreading of biological fluids, osseointegration, and bone-implant contact (BIC) strength. Bioactivity is a feature of surface chemistry and topography. This study indicated that surfaces subjected to laser texture have higher osseointegration. <sup>(12)</sup> Surface roughness is influenced by cell migration and widespread availability, leading to a quicker BIC. <sup>(13)</sup> It is made explicitly clear that only by changing or adjusting the surface texture, specifically the roughness (0.44 to 8.68 nm) of titanium implants, preferred results such as bone-implant interaction, retrieval torque values, tissue reaction, and biocompatibility can be attained. <sup>(14,41)</sup>

Current research emphasizes the use of CO<sub>2</sub> laser processing for the development of microstructures on titanium surfaces and the characterization of these structures by performing surface analysis procedures.

## 2. Materials and Methods

### 2.1. Specimen preparation:

Thirty discs with dimensions of 30 mm in diameter and 5 mm in thickness were prepared from commercially pure titanium (grade 2) rod utilizing a lathe cutting device (DREMEL MULT PRO., model 394, AMC- Denmark). <sup>(15)</sup> The discs were ground on silicon carbide paper (Strurer, Denmark) with 1000 grit at 250 rotations per minute (rpm) for two minutes for each grinding step.

Ultrasonic cleaning was performed sequentially in 90% acetone, 90% ethyl alcohol, and deionized water using an ultrasonic cleaning device (CODY/CD-2800, China) to eliminate particles and contaminants from the polished specimens. This procedure was performed for 15 min. Then these specimens were dried in a hot-air oven (MTI Corporation, USA) for 15 min at 100 °C.

## 2.2. Direct Laser Texturing (DLT):

The specimen's substrate surface was scanned by a head of laser device (Wanchai, JAFFETEC, Hong Kong, China) to generate the required strut hatch network design, which was stored in the device memory. The laser beam with power of 20 Watt focused on a metallic substrate to create a molten metallic pool on the surface that melted and solidified. This process was continued in an identical manner until the entire part of the 3 - dimensional CAD model was produced on the surface of the specimen substrate.

All specimens were ultrasonically disclosed for 1h in acetone (SIGMA-ALDRICH, Germany, expire date: 2024) and 99.8% anhydrous ethanol (SIGMA-ALDRICH, Germany, expire date: 2024) baths at room temperature<sup>(16)</sup>, and rinsed with de-ionized water for 1h after of each solvent.<sup>(17)</sup>

## 2.3. Continuous laser beam carbon dioxide (CNC-CO<sub>2</sub>) laser system.

Texturing titanium discs was performed with a continuous laser beam carbon dioxide (CNC - CO<sub>2</sub>) red laser system (Wanchai, JAFFETEC, Hong Kong, China) at a fundamental wavelength of  $\lambda=10600$  nm. The laser beam was focused onto the surface of the samples utilizing an 80 mm diameter zinc selenide lens (ZnSe) with a 190 mm focal length. The pulse power in the range of 34 W was used for processing, lower than this range resulted in no surface texturing. On the other hand, power of more than 34 W leads to

complete reflection of the laser from the titanium substrate surface.

## 2.4. Morphological surface analyses

### 2.4.1. Scanning Electron Microscopy

Before the scanning procedure, all the specimens were coated with gold. The process started with sputtering for two cycles (every 20 s) at 0.12 mA and 30 mbar with a thin layer of gold to decrease the electric charge of SEM samples and achieve the maximum possible value of imaging.<sup>(18)</sup> The microstructure and surface morphology of the control and laser-textured titanium samples were characterized using scanning electron microscopy (FEI-company, model S-50, Netherlands inspect) at various resolutions (100, 200, 500, 1000, 2000, 5000, 10000, and 20000X)<sup>(19)</sup> and an accelerating voltage of 20 kV for the entire surface.<sup>(20,21)</sup>

### 2.4.2. Elemental energy-dispersive spectroscopy (EDS) analysis

X-ray excitation of the specimens was accomplished for the evaluation of each unique element. Distinctive X-rays of the elements present in the sample were emitted after exposure to high-intensity X-rays, and the detector picked them. After that, the signals from the detector were examined. Every distinct element has an atomic structure that allows the emission of electromagnetic spectrum to have a distinct set of peaks for the chemical characterization of specimens.<sup>(22)</sup>

In order to improve surface conductivity, the samples were sputtered with a thin layer of platinum (white gold) using sputtering equipment prior to detection.<sup>(15)</sup> To ascertain the level of surface contamination on titanium, a unique phase comparison of laser-textured titanium discs was carried out.<sup>(23)</sup>

A 15 kV acceleration voltage, a 12 mm operating distance, and a 60-second EDS series duration were the

characteristics that were employed. The EDS device (Bruker Company-Germany, X-Flash, Model-6L) was provided with a software package for recording the spectra, and manual measurements were made at a 3000X magnification.

For every disk, five to six randomly chosen points in the center (3 mm from the periphery) were examined. It was determined that concentrated electrons penetrated the sample to a depth of almost 1.5 mm. <sup>(24, 25)</sup>

#### 2.4.3. X-ray diffraction analysis

By using X-ray diffraction, the crystalline structures of the laser-textured and control specimens were examined and contrasted. A D2 Phaser diffractometer (XRD-Bruker, Germany, 2010) operating at 40 kV and 40 mA, which used Ni-filtered Cu K $\alpha$  radiation ( $\lambda = 1.5418 \text{ \AA}$ ) to identify the constituent phases of the disc specimens was used to detect phase <sup>(26)</sup> from 20 and 80 using a 50 s/min counting rate. The surface layer's calculated detectable depth is about 0.2 mm <sup>(18)</sup>, even though the complex macro- and micro-texture structures in XRD records should prevent quantitative interpretation of the data. <sup>(20)</sup>

#### 2.4.4. Atomic force microscopy analysis

To acquire a 3-D surface profile, ten standardized points from each specimen

were chosen and scanned. The points were spaced 3 mm apart and measured from the disc's diameter center, starting at the outside edge on one side and moving toward the other. The software application Gwyddion was utilized to analyze these images and determine the common roughness (Ra) and peak-to-valley roughness (Rz). <sup>(20)</sup>

The titanium discs were cleaned in 99.8% ethanol (SIGMA-ALDRICH, Germany, expiration date: 2024) and placed on a platform so that the measuring plane was perpendicular to the profilometer before the surface topography was characterized. Sequential determinations of textured and untextured specimens were made beneath the contact surface profilometer (AA3000 Angstrom Advanced Inc., USA). <sup>(20)</sup>

#### 2.4.5. Microstructural and surface feature analyses

Discs micro structural evaluation was performed using an optical light microscope (Olympus, Japan). <sup>(27)</sup> The pictures were captured with Axioplan 2 and photograph module, with DC500 with software LEICA IM1000 V.4.0 (Leica Microsystems Imaging Solutions Ltd., Cambridge, United Kingdom). <sup>(27,28)</sup> An optical stereoscope has been extensively utilized to evaluate the homogeneity of the entire surface microstructure. <sup>(29)</sup>

### 3. Results

#### 3.1. Topography of the laser surface texturing

During the process of laser texturing with a 32 W CO<sub>2</sub> laser, the titanium surface exhibited a consistent and distinct rectangular pattern, as depicted in Figure (1), and evidenced by the high-definition images captured.

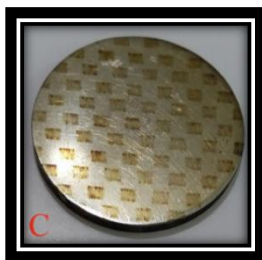


**Figure 1:** Topographic images: CO<sub>2</sub> textured titanium discs.

### 3.2. Optical Stereoscopy

Figure (2) presents the outcomes of examining the laser-textured surface through a photographic system linked to an optical stereoscope. The findings indicate a consistent pattern when observed under 40X magnification with a CO<sub>2</sub> laser.

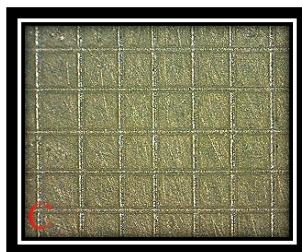


**Figure 2:** Optical microscope pictures X40 of CO<sub>2</sub> laser pattern.

### 3.3. Scanning Electron Microscopy (SEM):

Electron microscope was used to obtain images of the laser-textured surfaces. The images indicate that CO<sub>2</sub> laser texturing depicts a more orderly and less disorganized pattern, as displayed in Figure (3).

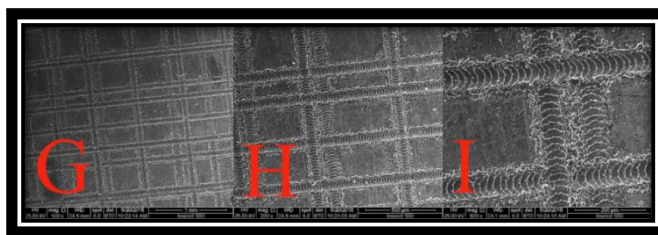


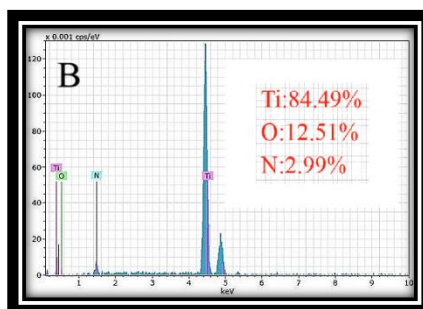
**Figure 3:** SEM micrographs of titanium surfaces textured using a CO<sub>2</sub> laser.

### 3.4. The Elemental analysis:

Table 1 presents the elemental concentrations of both the textured and untextured regions, as determined by the use of EDS for chemical characterization. It was observed that the primary chemical alteration occurring within the textured regions was the oxidation of titanium, a conclusion supported by the presence of oxides resulting in coloration within these regions. The energies of Ti, oxygen, and nitrogen at 4.50, 0.50, and 1.50 KeV respectively, are shown in Figure (4).

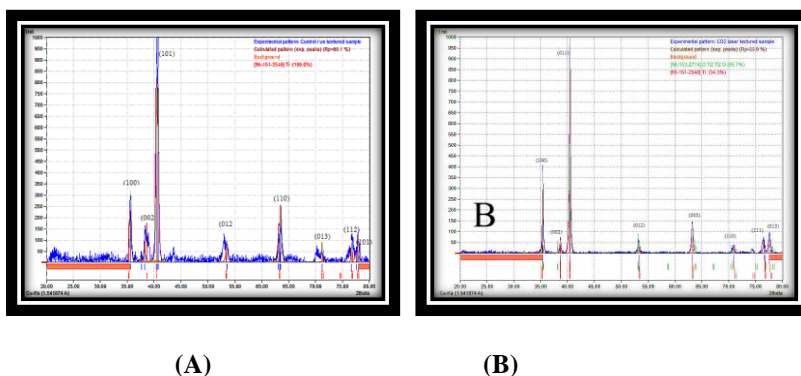
**Table 1:** Elemental analysis of titanium substrates textured by CO<sub>2</sub> laser texturing.

Element	[norm. wt.%]		[norm. wt.%]		
	Titanium 56 (L-series)	Oxygen 8 (K-series)	Nitrogen 7 (K-series)	Carbon 6 (K-series)	Sum of (K-series) wt%
Untextured Ti	89.56	10.43	0	0	100
CO <sub>2</sub> laser	84.49	12.51	2.99	0	100

**Figure 4:** EDS of titanium substrate textured by CO<sub>2</sub> laser.

### 3.5. X-ray diffraction (XRD) analysis

The quantity of untextured titanium material was 100 percent, as measured by X-ray diffraction (XRD), as shown in Figure (5: A). After laser texturing, the quantity was lower than that of the untextured material; however, it was slightly identical for all situations near 100 %. Additionally, XRD determined that the amount of TiO on the surfaces varied. It was confirmed that the percentage of TiO was a feature of heat input. The amount of oxide displayed a possible saturation of 65.7 % for CO<sub>2</sub> laser texturing, as shown in Figure (5: B).

**Figure 5:** A: XRD patterns of un-textured titanium disc, while B: XRD patterns of un-textured titanium disc.

### 3.6. Atomic force microscopy (AFM):

Starting with un-textured discs with values of arithmetic roughness Ra: 1.16 nm and the maximum height of the roughness profile Rz: 1.32 nm. The granulation distribution charts of the surface are shown in Figure (6: A). The untextured titanium surface appears to be uniform, with less roughness, minimal loss of parts of the surface, no noticeable cracks, and good granulation distribution. On the other hand, the

roughness profiles of the textures created by the CO<sub>2</sub> laser consisted of an array. The rounded tops are due to the re-solidification of the molten material, as shown in Figure (6: B). The roughness profiles created using the CO<sub>2</sub> laser are listed in Table (2).

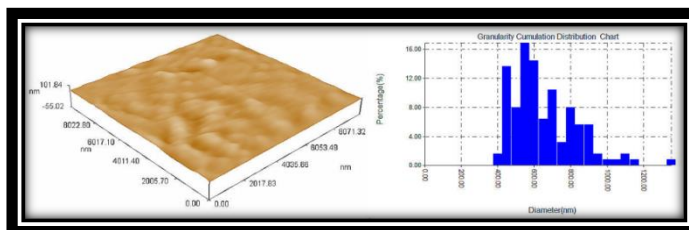


**Figure 6: A:** Analysis of surface roughness and distribution chart of untextured titanium discs.

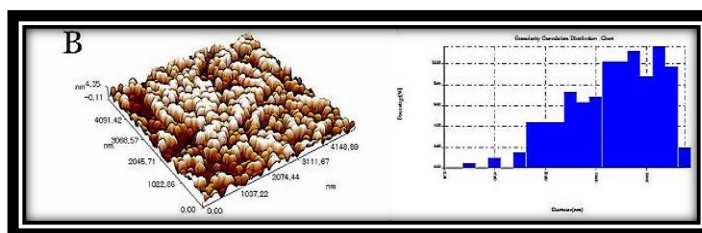


**Figure 6: B:** Analysis of surface roughness and distribution chart for textured titanium discs.

**Table 2:** Average values of Ra and Rz of titanium discs textured by CO<sub>2</sub> laser.

	Untextured	CO <sub>2</sub> -textured
<b>Ra</b>	1.16 nm	1.71 nm
<b>Rz</b>	1.32 nm	1.99 nm

#### 4. Discussion:

For CO<sub>2</sub> laser texturing, the high power of the laser implies light absorption that causes a temperature to rise on the external surface layer, melting, or vaporization.<sup>(29, 30)</sup> Which leads to a noticeable crater formation with slightly different colors (brown) which were regular, with optimum dimensions?<sup>(31, 32)</sup> This is a direct consequence of different oxide films formed on the surface of the textured areas.<sup>(33)</sup>

When comparing images of un-textured titanium surfaces with those acquired after texturing. Un-textured titanium discs have a smooth surface; with only significant

faults of linear lines that emerge because of manufacturing and processing. For the SEM examination, the titanium laser-textured surface exhibited consistent patterns throughout the entire surface. Exhibiting microscopic characteristics that play a significant role in expanding the external surface area. In contrast, there were only scratching structures on the entire untextured titanium surface, and there were no microscopic characteristics. This implies that the untextured surface has little impact on the surface area compared with the laser-textured sites.<sup>(34)</sup>

Also, the EDS spectrum revealed that there was an absolute improvement in the concentration of titanium oxide in

comparison with un-textured sites.<sup>(35)</sup> The results show that oxygen was present in the textured regions, whereas it was absent in the untextured sites, which have no oxidizing activity. The structures formed through laser texturing mainly consist of a large part of TiO rutile phase, which can be related to the multi-oxidation process of the tetragonal rutile structure of TiO.<sup>(36)</sup> Also, the EDS assessment demonstrated that Ti, O, and C were the only three components observed in the laser-textured titanium surfaces. While only titanium was discovered on the un-textured surface, indicating that this surface has a thickened oxide layer compared to the un-textured surface.<sup>(37,38)</sup>

The roughness of the textured area simply reflects the increase in power during texturing which leads to an increase in roughness owing to the modification of the texture dimensions; this effect of an increase in roughness occurred with 32 W of CO<sub>2</sub> texturing, with parallel micro-features noted, as they were parallel to the direction of the laser translation, but it was slightly moderate because of the high superposition of pulses.<sup>(39)</sup> In addition, a lower power tends to melt the surface with thermo-capillarity, causing a net change in surface roughness.<sup>(40,41)</sup>

## 5. Conclusion:

The CO<sub>2</sub> laser can be used as an effective tool for texturing titanium implant surface. This laser can be used as a continuous laser beam for texturing the surface of titanium with better surface characterization outcomes.

## Conflict of interest

The authors reported that they have no conflicts of interest.

## References

1. Spencer, N.D. (2011). Tailoring surfaces: Modifying surface composition and structure for applications in tribology, biology, and catalysis. Singapore; Hackensack, NJ: World Scientific.
2. Sonsaree, S., Asaoka, T., Jiajitsawat, S., Aguirre, H. and Tanaka, K. (2017). VCHP-ORC power generation from low-grade industrial waste heat combined with solar water heating system: Power generation and CO<sub>2</sub> emission in the industrial estate of Thailand. Cogent Engineering, 4(1).
3. Lee, H., Lim, C.H.J., Low, M.J., Tham, N., Murukeshan, (2017). Lasers in additive manufacturing: A review. International Journal of Precision Engineering and Manufacturing-Green Technology, 4(3), pp.307–322.
4. Mayer, A. (2012). Laser materials processing market has reached a record high. Advanced Optical Technologies, 1(5).
5. Markovic, V., Rohrbacher, A., Hofmann, P., Pallmann, W., Pierrot, (2015). 160 W 800 fs Yb: YAG single-crystal fiber amplifier without CPA. Optics Express, 23(20), p.25883.
6. Li, W.D., Yan, C.P., Wu, Y., Weng, Z.B., Yin, F.Z., (2014). Osteoblasts proliferation and differentiation stimulating activities of the main components of Fructus Psoraleae corylifoliae. Phytomedicine, 21(4), pp.400-405.



7. Figiel, P. (2015). Ocena wpływu przygotowania powierzchni na właściwości korozyjne kompozytów cermetalicznych w osnowie stali AISI 316L. *INŻYNIERIA MATERIAŁOWA*, 1(6), pp.161–164.
8. Qin, L., Lin, P., Zhang, Y., Dong, G., and Zeng, Q. (2013). Influence of surface wettability on the tribological properties of laser textured Co-Cr-Mo alloy in aqueous bovine serum albumin solution. *Applied Surface Science*, 268, pp.79–86.
9. Hu, T., Hu, L., and Ding, Q. (2012). Effective solution for the tribological problems of Ti-6Al-4V: Combination of laser surface texturing and solid lubricant film. *Surface and Coatings Technology*, 206(24), pp.5060–5066.
10. Vilar, R. (2016). *Laser surface modification of biomaterials: techniques and applications*. Amsterdam: Elsevier/Woodhead Publishing.
11. Pflieger, W., Kumari, R., Besser, H., Scharnweber, (2015). Laser surface textured titanium alloy (Ti-6Al-4V): Part 1-Surface characterization. *Applied Surface Science*, 355, pp.104-111.
12. Chen, J., Bly, R.A., Saad, M.M., AL-khodary, M.A., (2011). In-vivo study of adhesion and bone growth around implanted laser groove/RGD-functionalized Ti-6Al-4V pins in rabbit femurs. *Materials Science and Engineering: C*, 31(5), pp.826–832.
13. Heimann, R.B., and Lehmann, H.D. (2015). Bioceramic coatings for medical implants: trends and techniques. Weinheim, Germany: Wiley-Vch Verlag GmbH & Co. Kga.
14. Huang, C-C, Jiang, C-C, Hsieh, C-H, Tsai, C-J & Chiang, H (2015), Local bone quality affects the outcome of prosthetic total knee arthroplasty, *Journal of Orthopaedic Research*, vol. 34, no. 2, pp. 240–248.
15. Li, Y., Yang, W., Li, X., Zhang, X., Wang, C., Meng, X., (2015). Improving Osteointegration and Osteogenesis of Three-Dimensional Porous Ti6Al4V Scaffolds by Polydopamine-Assisted Biomimetic Hydroxyapatite Coating. *ACS Applied Materials & Interfaces*, 7(10), pp.5715–5724.
16. Sidambe, A. (2014). Biocompatibility of Advanced Manufactured Titanium Implants—A Review. *Materials*, 7(12), pp.8168–8188.
17. Akinlami, J.O. (2012). Reflection coefficient and optical conductivity of gallium nitride GaN. *Semiconductor Physics Quantum Electronics and Optoelectronics*, 15(3), pp.281–284.
18. Shruti, S., Andreatta, F., Furlani, E., Marin, E., (2016). Cerium, gallium, and zinc-containing mesoporous bioactive glass coating deposited on titanium alloy. *Applied Surface Science*, [online] 378, pp.216–223.
19. Ramakrishnaiah, R., AL kheraif, A.A., Mohammad, A., (2017). Preliminary fabrication and characterization of electron beam

- melted Ti-6Al-4V customized dental implant. *Saudi Journal of Biological Sciences*, 24(4), pp.787–796.
20. Wang, M., Wu, Y., Lu, S., Chen, T., Zhao, Y., Chen, H. (2016). Fabrication and characterization of selective laser melting printed Ti-6Al-4V alloys subjected to heat treatment for customized implant design. *Progress in Natural Science: Materials International*, 26(6), pp.671–677.
  21. Tamaddon, M., Samizadeh, S., Wang, L., Blunn, (2017). Intrinsic Osteoinductivity of Porous Titanium Scaffold for Bone Tissue Engineering. *International Journal of Biomaterials*, pp.1–11.
  22. Zhang, J., Han, H., Tian, W., Lv, L., Wang, Q. and Wei, Z. (2013). Diode-pumped 88-fs Kerr-lens mode-locked Yb:Y<sub>3</sub>Ga<sub>5</sub>O<sub>12</sub> crystal laser. *Optics Express*, 21(24), p.29867.
  23. Busuioc, C., Voicu, G., Zuzu, I.D., Miu, D., Sima, C., (2017). Vitroceramic coatings deposited by laser ablation on Ti-Zr substrates for implantable medical applications with improved biocompatibility. *Ceramics International*, 43(7), pp.5498–5504.
  24. Kawai, T., Takemoto, M., Fujibayashi, S., Akiyama, H., (2014). Osteoinduction on Acid and Heat Treated Porous Ti Metal Samples in Canine Muscle. *PLoS ONE*, 9(2), p.e88366.
  25. Bououdina, M., Rashdan, S., Bobet, J.L. and Ichiyanagi, Y. (2013). *Nanomaterials for Biomedical Applications: Synthesis, Characterization, and Applications*. *Journal of Nanomaterials*, [online] 2013, pp.1–4.
  26. Yang, D.F. (2012). Pulsed Laser Deposition of Pseudocapacitive Metal Oxide Thin Films for Supercapacitor Applications. *Materials Science Forum*, 706–709, pp.884–889.
  27. Amin Yavari, S., Ahmadi, S.M., Van der stok, J., (2014). Effects of bio-functionalizing surface treatments on the mechanical behavior of open porous titanium biomaterials. *Journal of the Mechanical Behavior of Biomedical Materials*, 36, pp.109–119.
  28. Govindarajan, P., Khassawna, T., Kampschulte, M., (2013). Implications of combined ovariectomy and glucocorticoid (dexamethasone) treatment on mineral, microarchitectural, biomechanical, and matrix properties of rat bone. *International Journal of Experimental Pathology*, 94(6), pp.387–398.
  29. N. Ahmed Hussein, Ali, and Raghdaa K Jassim. (2019). “Application of Continuous Wave ND-YAG Laser for Improving Surface Roughness of Cp-Titanium.” *Indian Journal of Forensic Medicine & Toxicology* 13 (4): 1096–1100.
  30. Wen, M., Wen, C., Hodgson, P. and Li, Y. (2012). Thermal oxidation behavior of bulk titanium with the nanocrystalline surface layer. *Corrosion Science*, 59, pp.352–359.

31. Cei, S., Karapetsa, D., Aleo, E. and Graziani, F. (2015). Protein Adsorption on a Laser-Modified Titanium Implant Surface. *Implant Dentistry*, p.134-141.
32. Adams, D.P., Murphy, R.D., Saiz, D.J., (2014). Nanosecond pulsed laser irradiation of titanium: Oxide growth and effects on underlying metal. *Surface and Coatings Technology*, 248, pp.38–45.
33. Vázquez-Martínez, J.M., Salguero, J., Botana, F.J., (2013). Metrological Evaluation of the Tribological Behavior of Laser Surface Treated Ti6Al4V Alloy. *Procedia Engineering*, 63, pp.752–760.
34. Horn, A., Kalmbach, C.-C., Moreno, J.G., Schütz, V., (2012). Laser-Surface-Treatment for Photovoltaic Applications. *Physics Procedia*, 39, pp.709–716.
35. Erdoğan, M., Öktem, B., Kalaycioğlu, H., Yavaş, S., (2011). Texturing of titanium (Ti6Al4V) medical implant surfaces with MHz-repetition-rate femtosecond and picosecond Yb-doped fiber lasers. *Optics Express*, 19(11), p.10986.
36. Szmukler-moncler, S., Bischof, M., Nedir, R. and Ermrigh, M. (2010). Titanium hydride and hydrogen concentration in acid-etched commercially pure titanium and titanium alloy implants: a comparative analysis of five implant systems. *Clinical Oral Implants Research*.
37. Salguero, J., Batista, M., Sanchez Galindez, (2011). An XPS Study of the Stratified Built-up Layers Developed onto the Tool Surface in the Dry Drilling of Ti Alloys. *Advanced Materials Research*, 223, pp.564–572.
38. Vera, M.L., Avalos, M.C., Rosenberger, M.R., (2017). Evaluation of the influence of texture and microstructure of titanium substrates on TiO<sub>2</sub> anodic coatings at 60 V. *Materials Characterization*, 131, pp.348–358.
39. N Ahmed Hussein, Ali, and Raghdaa K Jassim. (2020). “Development of Hatching Microstructure on Cp-Titanium Surface by Fiber Optic Laser Processing.” *Indian Journal of Public Health Research & Development* 11 (4): 2000–2006.
40. Cicek, S., Karaca, A., Torun, I., Onses, M.S. and Uzer, B. (2019). The relationship of surface roughness and wettability of 316L stainless steel implants with plastic deformation mechanisms. *Materials Today: Proceedings*, 7, pp.389–393.
41. Ahmed Hussain, Ali Nima, and Raghdaa Kareem Jassim. 2019. “The Role of Laser Texturing and Coating of Commercial Pure Titanium Implants with Silicon Dioxide and Gallium Nitrate in Enhancing Osseointegration in Osteoporosis (in Vitro and in Vivo Study).” PhD Thesis, College of Dentistry at the University of Baghdad.